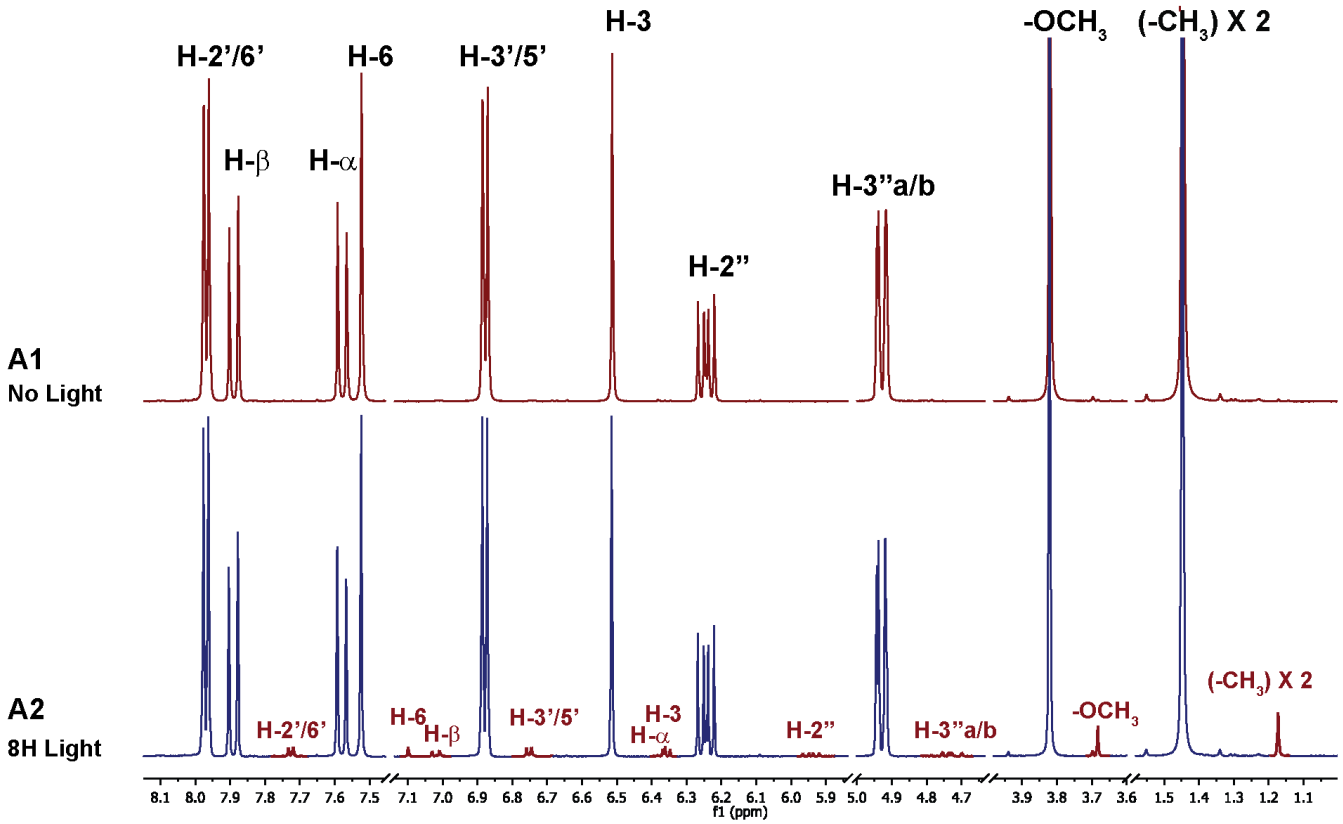

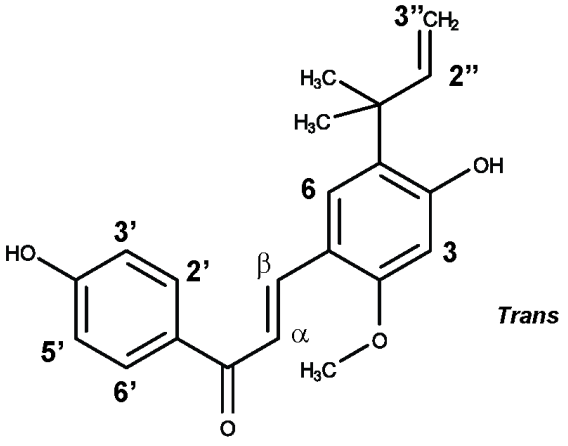

Trans

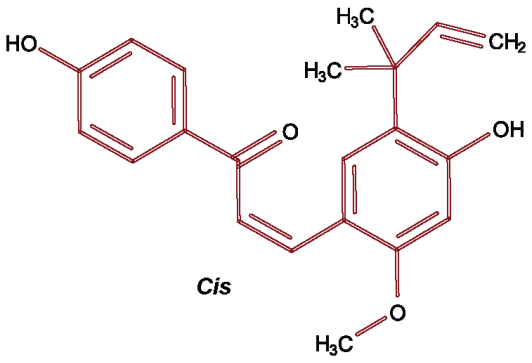

Cis

Figure S1. Proton NMR (600 MHz, DMSO-d_6) analysis of licochalcone A showing the *E* to *Z* isomerization during 8-hour exposure to laboratory light. A1) Sample protected from light and containing only *trans*-licochalcone A; and A2) sample incubated for 8-hour under light, thus containing 3% cis isomer (Simmler et al, 2017).

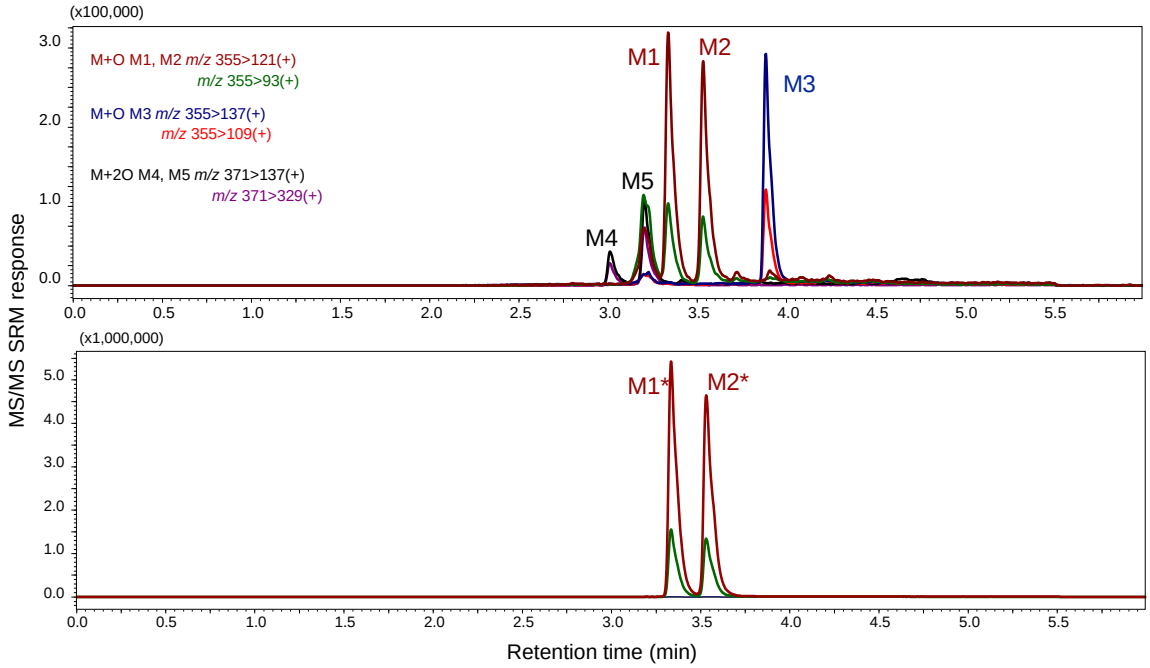

Figure S2A. UHPLC-MS/MS chromatograms of licochalcone A phase I metabolites (top) and compounds in a *G. inflata* fraction showing identical retention times for M1 and M1* as well as M2 and M2*.

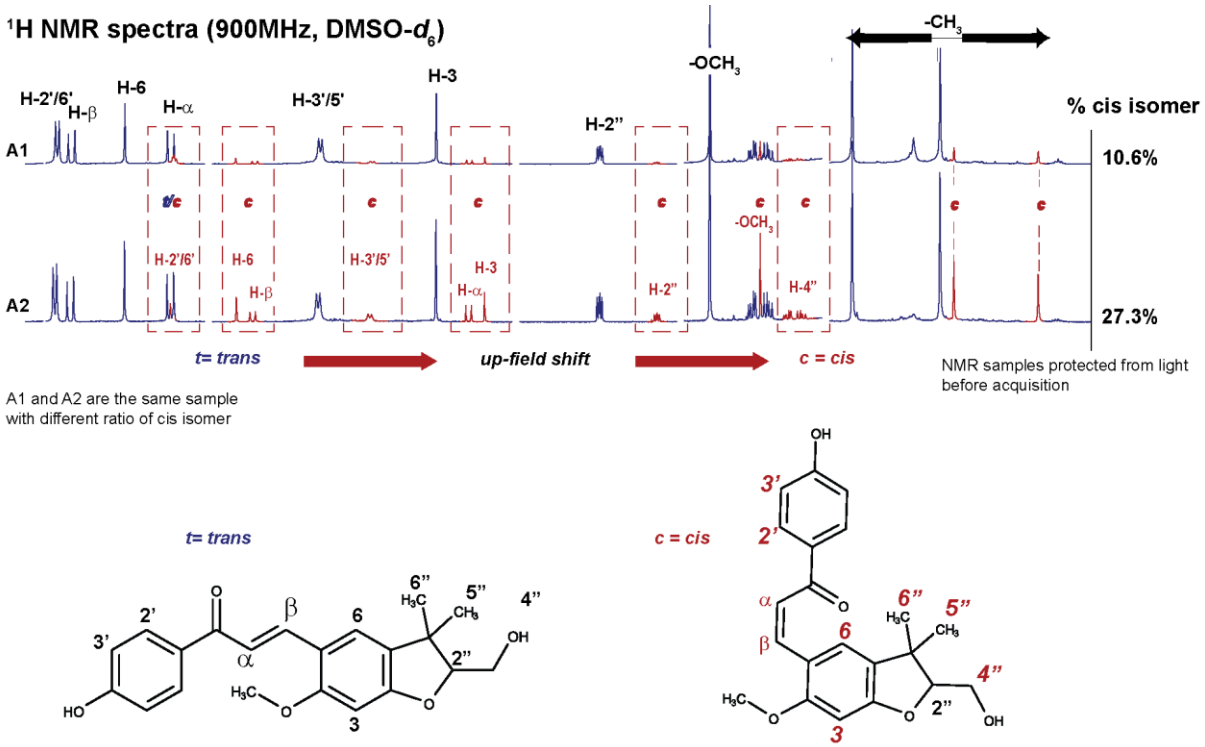

Figure S2B. Proton NMR analysis (900 MHz, DMSO-d_6) of *E* to *Z* isomers (M1* and M2*) of *G. inflata* secondary metabolite 3-(2-(hydroxymethyl)-6-methoxy-3,3-dimethyl-2,3-dihydrobenzofuran-5-yl)-1-(4-hydroxyphenyl)prop-2-en-1-one, which are identical to the phase I licochalcone A metabolites M1 and M2 (Simmler et al, 2017).

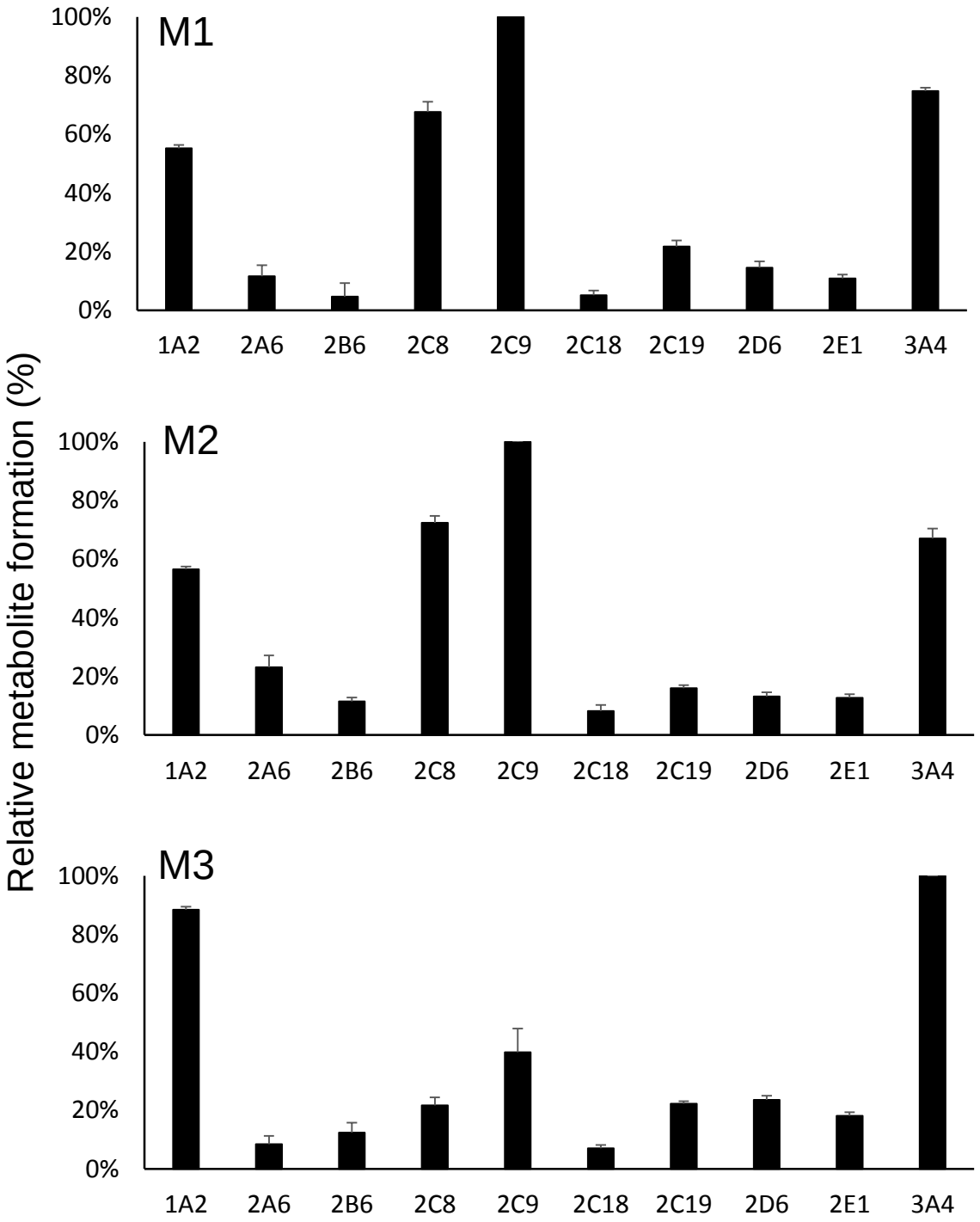

Figure S3 Relative formation of licochalcone A phase I metabolites by recombinant cytochrome P450 enzymes (5 pmol each). Each recombinant enzyme was incubated with licochalcone A and NADPH, and formation of licochalcone A metabolites M1, M2 and M3 were compared using UHPLC-MS/MS. Data were multiplied by the mean specific content of corresponding cytochrome P450 enzymes in human liver microsomes to normalize their contributions. (Mean ± S.E.; n=3).

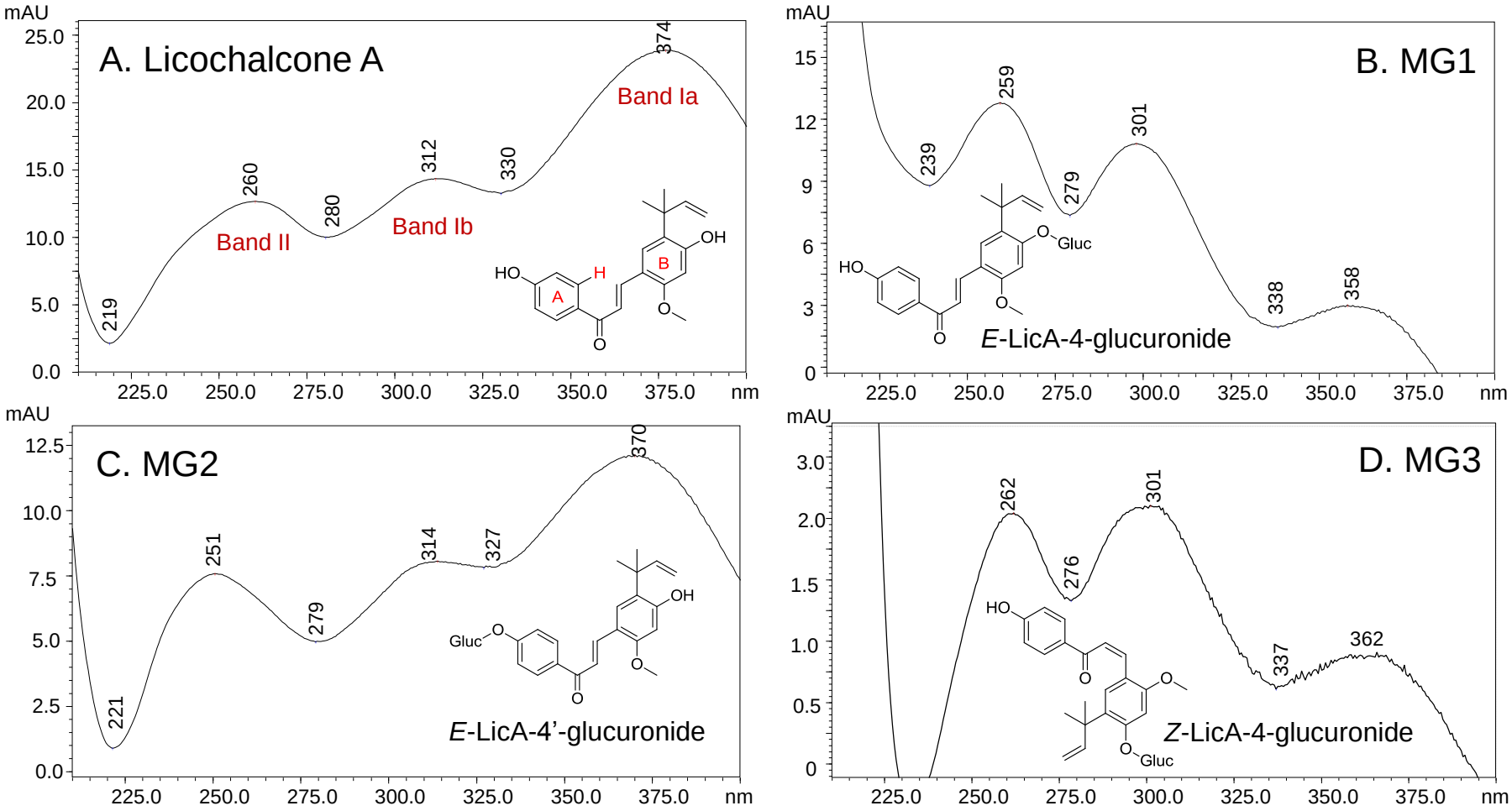

Figure S4. UV spectra of A) licochalcone A; and its monoglucuronides; B) MG1; C) MG2; and D) MG3. Band I (300-380 nm) and Band II (240-280 nm) are associated with the B-ring and A-ring, respectively.

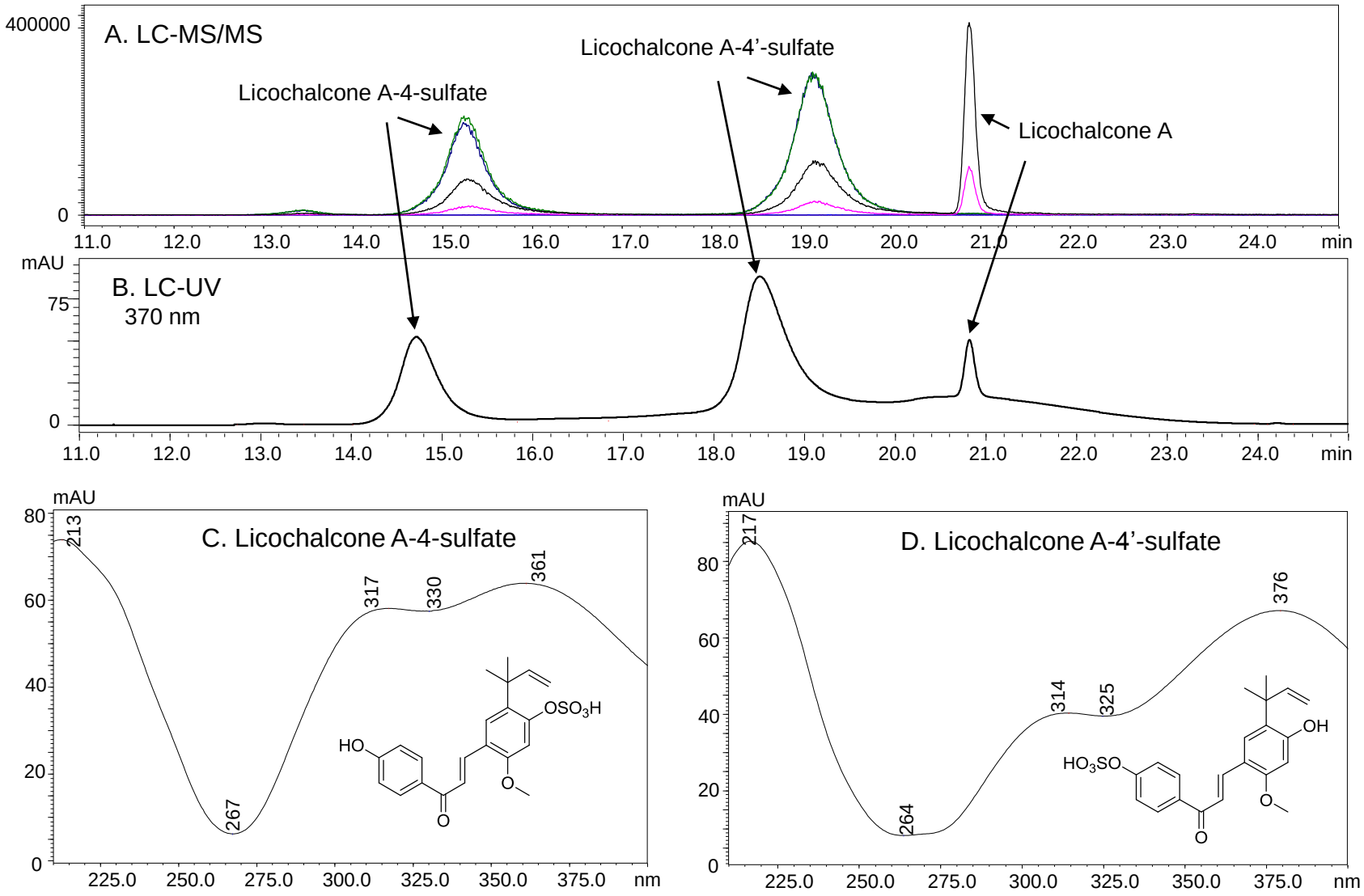

Figure S5. A) LC-MS/MS chromatograms of licochalcone A and its two synthetic monosulfates. B) LC-UV chromatogram of licochalcone A and its monosulfate conjugates. C) UV spectrum of licochalcone A-4-sulfate; and (D) UV spectrum of licochalcone A-4'-sulfate.

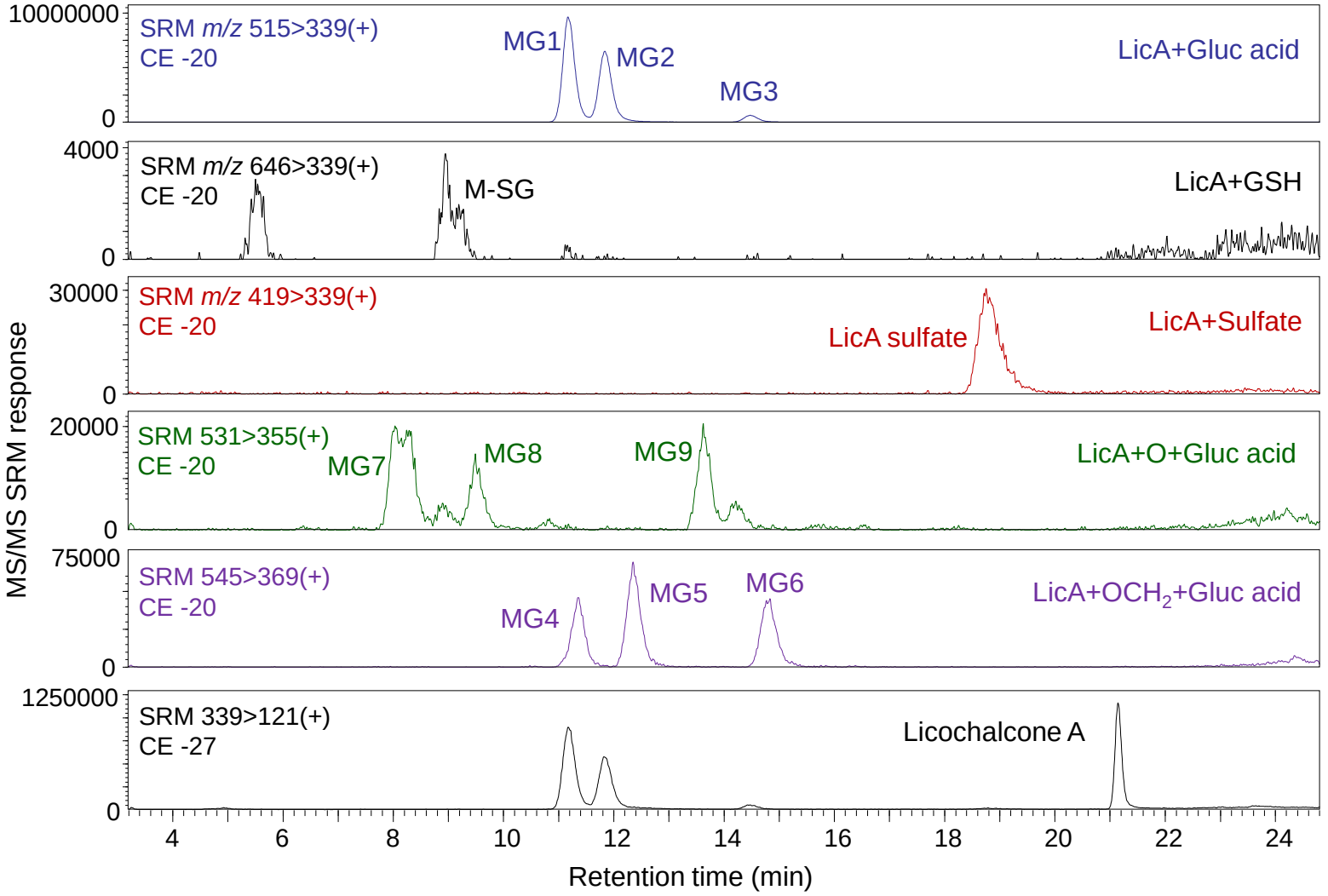

Figure S6. Positive ion UHPLC-MS/MS chromatograms of licochalcone A metabolites formed during incubation with human hepatocytes.

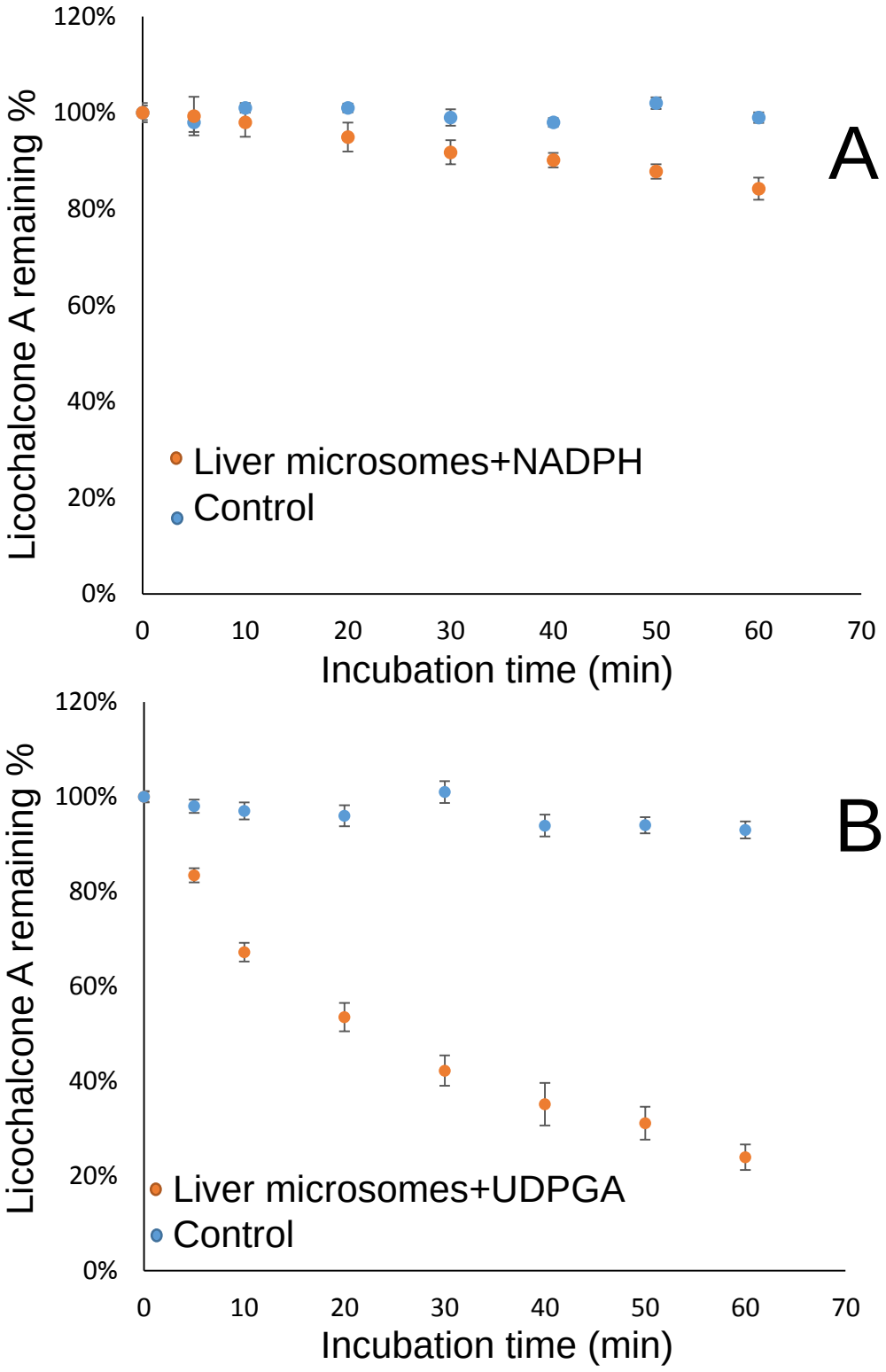

Figure S7. Metabolic stability of licochalcone A during incubation with human liver microsomes and (A) NADPH for phase I metabolism; and (B) UDPGA for phase II glucuronidation. The amount of licochalcone A remaining at each time point was determined by LC-MS/MS. Incubation without microsomes was used as a negative control. Data are expressed as Mean±S.D.

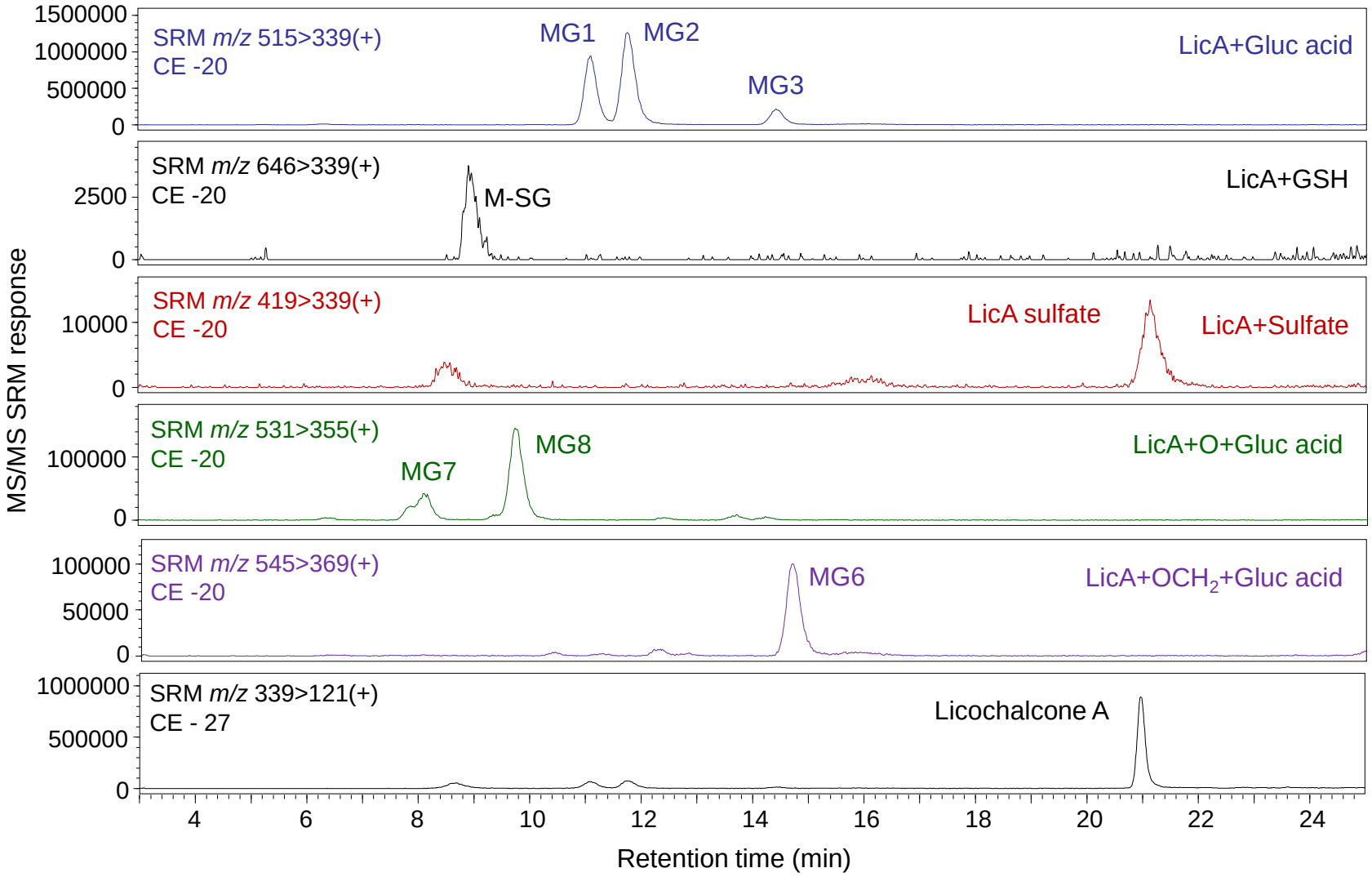

Figure S8. Positive ion UHPLC-MS/MS chromatograms of licochalcone A metabolites in rat serum. (CE = collision energy)

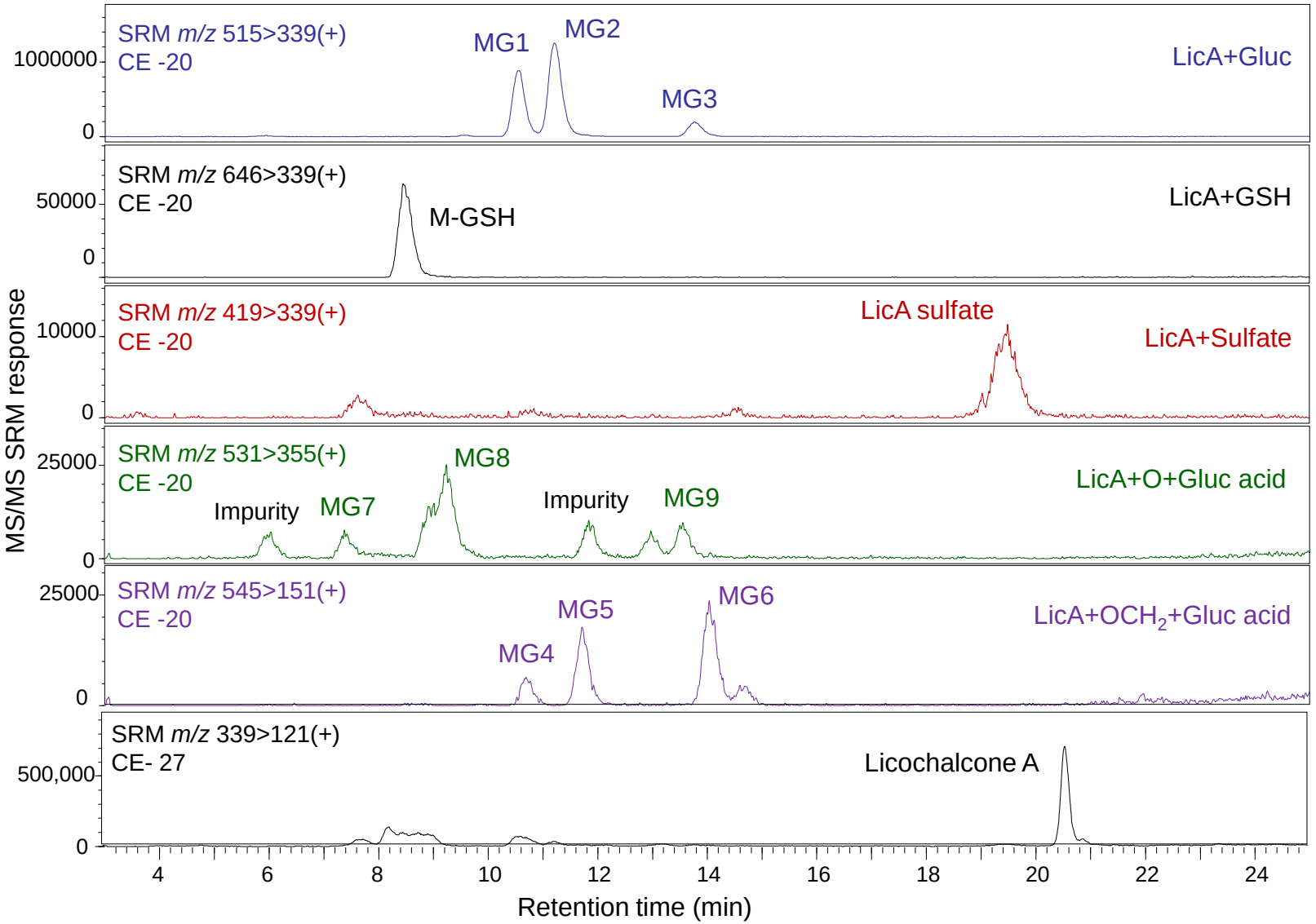

Figure S9. Positive ion UHPLC-MS/MS chromatograms of licochalcone A metabolites in rat liver.

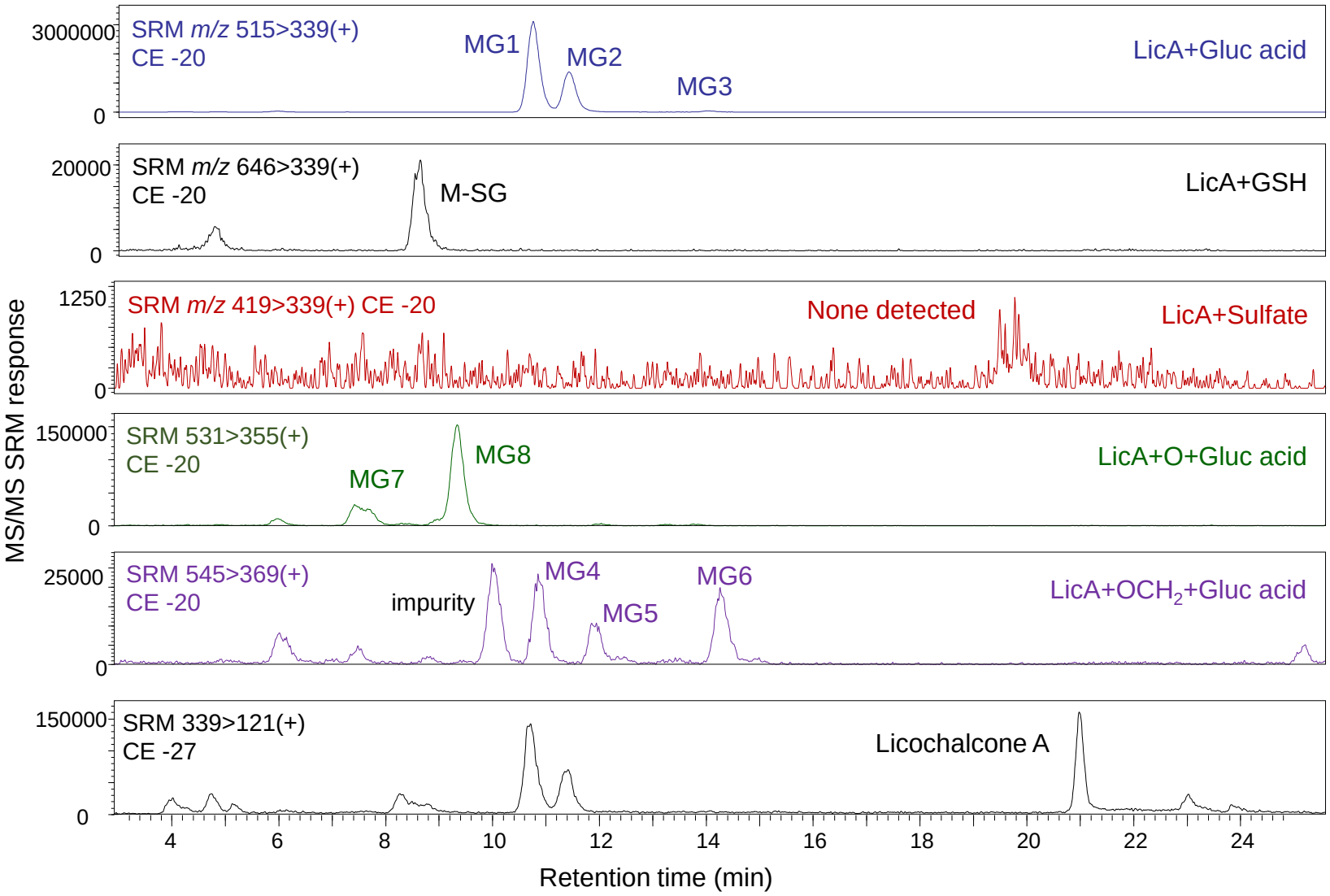

Figure S10. Positive ion UHPLC-MS/MS chromatograms of licochalcone A metabolites in rat mammary tissue.